www.elsevier.com/locate/csr

Velocity and sediment surge: What do we see at times of very shallow water on intertidal mudflats?

Qian Zhang, Zheng Gong, Changkuan Zhang, Ian Townend, Chuang Jin, Huan Li

PII: S0278-4343(15)30110-2
DOI: http://dx.doi.org/10.1016/j.csr.2015.12.003
Reference: CSR3325

To appear in: *Continental Shelf Research*

Received date: 24 April 2015
Revised date: 7 December 2015
Accepted date: 14 December 2015

Velocity and sediment surge: what do we see at times of very shallow water on intertidal mudflats?

Qian Zhang[a], Zheng Gong [1a], Changkuan Zhang[b], Ian Townend[c], Chuang Jin[b], Huan Li[b]

[a]*State Key Laboratory of Hydrology-Water Resources and Hydraulic Engineering, Hohai University, Nanjing 210098, China*
[b]*College of Harbour, Coastal and Offshore Engineering, Hohai University, Nanjing 210098, China*
[c]*University of Southampton, Southampton, U.K.*

Abstract

A self-designed "bottom boundary layer hydrodynamic and suspended sediment concentration (SSC) measuring system" was built to observe the hydrodynamic and the SSC processes over the intertidal mudflats at the middle part of the Jiangsu coast during August 8-10, 2013. Velocity profiles within 10 cm of the mudflat surface were obtained with a vertical resolution as fine as 1 mm. An ADCP was used to extend the profile over the full water depth with a resolution of 10 cm and the vertical SSC profile was measured at intervals using Optical Backscatter Sensors (OBS). At the same time, water levels and wave conditions were measured with a Tide and Wave Recorder. Measured data suggested that the vertical structure of velocity profiles within 10 cm above the bed maintains a logarithmic distribution during the whole tidal cycle except the slack-water periods. Shallow flows during both the early-flood period and the later-ebb period are characterized by a relatively

[1]Corresponding author. Tel: +86 13705187083; fax: +86 025 8378 7340. *E-mail address*: gongzheng@hhu.edu.cn

large vertical velocity gradient and a “surge” feature. We conclude that the very shallow water stages are transient and may not contribute much to the whole water and sediment transport, while they can play a significant role in the formation and evolution of micro-topographies on tidal flats.

Keywords: mudflats, field investigation, very shallow water, velocity surge, suspended sediment concentration surge, micro-topography

1. Introduction

Mudflats are shallow areas characterized by fine cohesive sediment supplied from adjacent rivers, estuaries and coasts. They are found worldwide under a variety of climate, hydrodynamic and sedimentologic conditions. Some of the well-documented examples include the east coast of China (Ren, 1986; Wang and Wall, 2010), the Severn Estuary of the UK (Williams et al., 2008; Carling et al., 2009), the Amazon Estuary of South America and Fly River mouth of Oceania (Allison et al., 1995; Walsh and Nittrouer, 2004), the northwest coast of America (Fagherazzi and Mariotti, 2012; Nowacki and Ogston, 2013), and the west coast of the Netherlands (Kleinhans et al., 2009). Mudflats are important components of coastal and estuarine systems for their socio-economic and ecological values (e.g., wave damping, coastal protection, and providing habitats to wildlife).

China has extensive mudflat resources which mainly distribute along the bay area, flank Deltas of big estuaries and the middle coast area, accounting for approximately a quarter of the country’s total coastline. The widest and the most concentrated mudflats are located in Jiangsu province, with a length of approximately 900 km (from north to south) and an area of about 5000

km^2 above the nationally defined 0 m contour line (i.e., the 1985 National Height Datum, about 0.3 m below the local mean tide level). These mudflats exhibit a range of erosional and depositional dynamics, coastal ecosystem services, acting as the most quintessential and representative mudflats countrywide, and even worldwide (Yang, 2001). Such broad tidal flats are not only important wetland resources, but also a potential land resource that can ease the increasing pressure because of population growth. Therefore, detailed studies of tidal flats bear both scientific and practical significance, which can provide direct insights into the morphodynamic behavior of tidal flats and hence lay the foundation for numerical modeling and assist to the development of management strategies.

Narrow tidal creeks and widely bounded tidalflats are the two main geomorphic units of tidal flat systems. They have been extensively studied in terms of hydrodynamic characteristics, material transportation, sedimentary processes, and geomorphic processes (Whitehouse et al., 2000; Wang et al., 2006; Williams et al., 2008; Carling et al., 2009; Fagherazzi and Mariotti, 2012; Wang et al., 2012). Periodic emergence and submergence of tidal flats result in frequent variations in water depth, leading to a frequent occurrence of very shallow water conditions both temporally and spatially. This gives rise to a special hydrodynamic phenomenon as "velocity surge", which has been investigated and discussed by many researchers (e.g., Bayliss-Smith et al., 1979; Wang et al., 1999; Nowacki and Ogston, 2013).

Velocity surges (or pulses), defined as short-lived occurrences of elevated velocity (Nowacki and Ogston, 2013), usually associated with elevated suspended sediment concentration have been reported for both muddy and sandy tidal flats (Bayliss-Smith et al., 1979; Zhang, 1987). Early field studies of velocity surges were mainly carried out on salt marsh creeks during spring tides or storm surges (Bayliss-Smith et al., 1979; French and Stoddart, 1992). Later on, observations in fair weather indicated that well-defined velocity surges also occur during almost every tidal cycle in lower tidal channels (Wang et al., 1999; Nowacki and Ogston, 2013). Continuity arguments were used to explain this phenomenon (Boon, 1975; Bayliss-Smith et al., 1979; Pethick, 1980; Healey et al., 1981; Wang et al., 1999). Nowacki and Ogston (2013) deepened the theory and suggested that maintenance of continuity produces the velocity pulse, and the pulse magnitude is determined by tidal range. Moreover, bed morphology (e.g., large bed slope and small elevation) and a large hydraulic gradient between tidal flats and channels can enhance the velocity surge (Wang et al., 1999; Hughes, 2012).

The influence of velocity surges on the sediment dynamics and morphological evolution of channel-flat system is remarkable. Field observation in southern Willapa Bay suggested that pulses occupy only 8% of the deployment time but contribute up to 27% of the along-channel water transport and 35% of the suspended sediment transport (Nowacki and Ogston, 2013). At the end of the ebb, water flows off the marsh surface into the neighbouring creeks, leading to the formation of a convergent flow characterized by a large velocity in the creeks. The peak surge velocity can be comparable to the maximum velocity during flood or ebb. Accordingly, the induced suspended sediment concentration also shows a surge phenomenon and the peak value even reaches the magnitude observed during strong waves (Fagherazzi and Mariotti, 2012).

Compared to the channel-flat system, surges on only tidal flats have received much less attention. Although the magnitude is not as large as in the channel-flat system, the surge phenomenon has also been observed on tidal flats during certain hydrodynamic periods of "very shallow water" conditions, with a water depth (usually of the order of 10 cm) much smaller than the fully developed tide-induced bottom boundary layer which is vital to the flow-sediment interaction (Carling et al., 2009; Gao, 2010). At the initial stage of flood, a tidal front usually develops with a relatively large velocity (Xu et al., 1994; Xu and Wang, 1998; Gao, 2010). Under certain conditions even a "tidal bore" can occur, characterized by a front of breaking tidal wave associated with a strong flow in shallow water (Gao, 2010). The effective time of a tidal front or tidal bore is quite short; however, strong water turbulence can cause strong suspension of sediment. Deposited matter on the surface of tidal flats is disturbed and its consolidation process is disrupted, so that it is easier for the following tidal flow to re-suspend sediment (Xu and Wang, 1998).

In fact, even small velocity surges during "very shallow water" conditions on tidal flats play a considerable role on the formation and evolution of micro-topographies. Apart from the tidal front mentioned above, some researchers also pointed out the non-negligible role of sediment transport capacity of sheet flow during the latter period of the ebb tide, which can reshape the bed form in less than one hour (e.g., Gao, 2010). Although the water and sediment fluxes during these periods are small compared to the total tidal cycle, the surge process is valuable from a micro-topography viewpoint.

However, our understanding on shallow flow characteristics of tidal flats is still very limited, primarily because the water depth is often too small to arrange field measurements. Recently, with the development of more refined measurement techniques, as well as the awareness of the need for in-depth understanding of dominant processes on tidal flats, increasing investigations have been carried out in the shallow intertidal zone. Hydrodynamic and sediment processes as close as 20 cm to the bottom have been studied based on field observations (Trowbridge and Agrawal, 1995; Li et al., 2007; Williams et al., 2008; Fagherazzi and Mariotti, 2012). However, restricted by the field conditions and the blind area of instruments, there are few studies on the characteristics of hydrodynamic and sediment processes in very shallow water environments characterized by a water depth of the order of 10 cm. Previous observational data near the bottom with a vertical resolution is not sufficient for an in-depth understanding of the characteristic of the "surge" process (e.g., both velocity and suspended sediment concentration) in shallow water environments.

In this study, a field survey was carried out on intertidal mudflats and synchronous water depth-velocity-SSC data with a high vertical resolution were acquired. The overall aim of this study is to investigate the characteristics of flow and sediment processes during very shallow water periods, as well as their underlying physical mechanisms. To be more specific, our objectives include: (1) to describe flow and sediment conditions during initial flood and post ebb stages; (2) to explore the "surge" phenomena on tidal flats and compare with that in tidal creeks and (3) to examine the significance of surge phenomena on micro-topography formation. By addressing these research objectives, we hope to deepen the understanding on natural processes governing tidal flat morphodynamics.

2. Study Area

Muddy tidal flats in Jiangsu, occupy 95% of Jiangsu coastline, and are characterized by gentle slope, large width, small water depth, sufficient sediment supply and developed tidal creeks. The average width is 2-6 km and the slope is 0.01-0.03%. Our study was carried out on tidal flats in the south of Chuandong River, Yancheng City (Figure 1a), where the landscape shows clear zonation (Zhu et al., 1986). Hydrodynamic in this sea area is controlled by the radial tidal current field (Zhang et al., 1999). In the near-shore coastal area, the tide is irregular semi-diurnal (Gong et al., 2013). The average ratio of flood and ebb tide duration in the study area is about 0.73. The averaged tidal range is 3.68 m. The annual mean wind speed is 4-5 m/s while the probability of wave height less than 1 m is about 85% (Ren, 1986).

Field investigation was carried out during spring tide period from August 8 to 10, 2013, and lasted for three tidal cycles. Based on nine observation points arranged to monitor the elevation changes of the flat surface by our research team (S1-S9 in Figure 1b) (Gong et al., 2014), the station (star A, 33°03'6.60"N, 120°54'36.30"E) between S7 and S8 was chosen to set our observation instruments. The cross section of the nine stations and station A is illustrated in Figure 1c. Tidal flats here are broad, with no vegetation cover, and no tidal creek developed nearby. The median grain size of the substrate is approximately 79 μm, with the contents of sand, silt and clay occupying 69 %, 30 % and 1 %, respectively. During the observation period, the weather was fine, with a maximum wind speed of 6 m/s and a significant

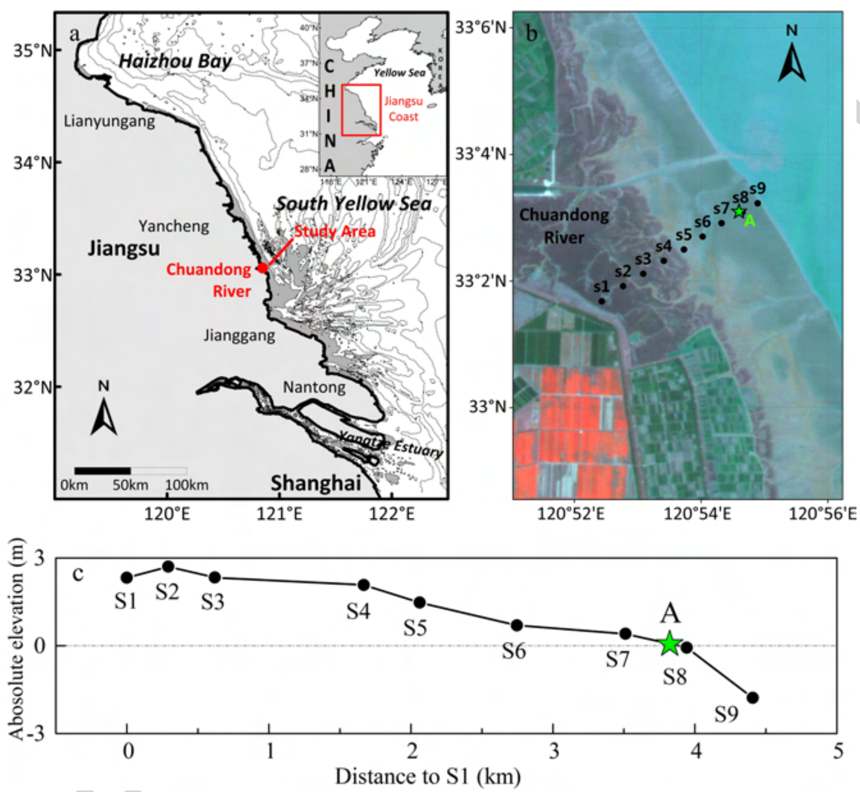

Figure 1: (a) Map of Jiangsu coast area, with study area indicated by red point; (b) Map of study area on mudflats in the south of Chuandong River, Yancheng City, with field survey station indicated by star A; (c) The cross shore profile of S1-S9.

wave height of 0.25 m. According to the formula proposed by (Nielsen, 1992), the thickness of the wave-induced bottom boundary layer is estimated as less than 1 cm, thus the wave effect is ignored in this paper.

3. Methods

3.1. Observation apparatus

A self-designed "bottom boundary layer hydrodynamic and suspended sediment concentration (SSC) measuring system" was used to acquire and record simultaneous water depth, high-resolution velocity and stratified SSC processes. The measuring system consists of the following instruments and components: a SonTek Vectrino Profiler, a 600 kHz RiverRay ADCP (RD INSTRUMENTS), Optical Backscatter Sensors (D & A Instruments OBS 5+ and OBS 3A, Campbell Scientific OBS 3+), a RBR Company Tide Wave Recorder-2050 (TWR for short), data acquisition and transmission device and power supply. The front view and top view of the frame is shown in Figure 2a-b. As some of the instruments were installed quite near the bottom, detailed views of the distance are shown in Figure 2c. To be more intuitive, Figure 2d shows a site photo of the measuring system and Figure 2e is the probe of "Vectrino Profiler".

"Vectrino Profiler" is the instrument used to capture velocity profile near the bottom with high precision and resolution. This velocity meter was fixed to the end of a 1 m-length cross bar which was attached to the main pole and settled 1.2 m high above the flat. The probe of the installed "Vectrino Profiler" was about 10 cm high over the flat surface (Figure 2c). Three-component velocity profiles were obtained within 4 cm to 7 cm range in front

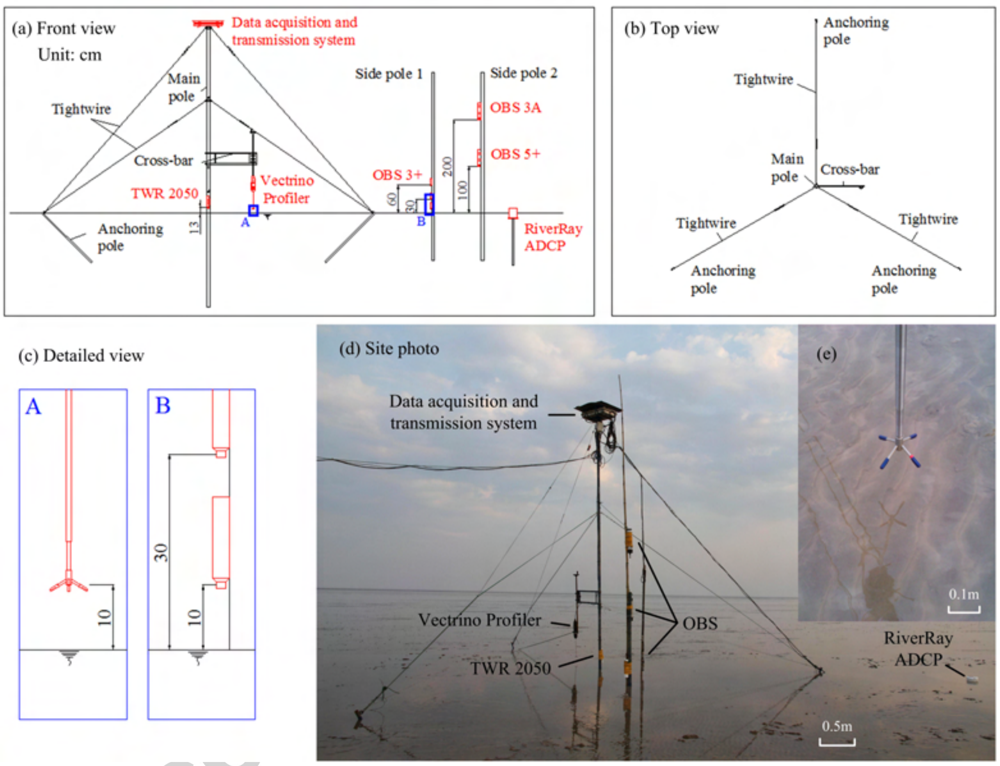

Figure 2: (a) Front view and (b) top view of the "bottom boundary layer hydrodynamic and suspended sediment concentration measuring system"; (c) detailed view of the height of instrument installation, with a unit of cm; (d) site photo of the measuring system; (e) the probe of "Vectrino Profiler".

of the probe with a sampling frequency of 25 Hz and a vertical resolution as fine as 1 mm. Notably, the bed elevation was always changing during the flood and ebb period. The "Vectrino Profiler" is able to record the distance from the transducer to the flat surface with a sampling frequency of 10 Hz. In this paper, the real-time height of the measured velocity is only used in the profile fitting, while the initial height of 3-6 cm above the flat surface is used in other statements of the velocity profile height in order to be uniform and easily understood.

Meanwhile, the velocity profile of the upper water column was measured by RiverRay ADCP. This instrument uses a phase array transducer, which has the advantage of reducing the blind zone and the interference of the instrument on the flow field compared with traditional ADCP. This instrument was buried upwards 5 m away from the main pole and the transducer surface was kept 10 cm higher than the mud surface. Measured layers are set by the instrument automatically according to the water depth with a minimum resolution of 10 cm, and the first measured layer of velocity is 25 cm away from the transducer. Combined with velocity profiles provided by "Vectrino Profiler", we can obtain velocity profiles extending to the whole water depth. The sampling frequency was set to be 1-2 Hz by the instrument automatically.

Suspended sediment concentration was measured by a group of five OBSs fixed to two side poles to the east of the main pole at heights of 10 cm, 30 cm, 60 cm, 1 m and 2 m above the mud surface. Water depth and wave heights were recorded continuously using TWR, the sampling intervals of waves and water depth are 10 min and 5 min, respectively.

3.2. SSC calibration

Turbidity calibration of OBSs was made using water samples taken in the field to convert the turbidity or the electric current data recorded directly by OBS into SSC. Limited by field conditions, it was difficult to get synchronistical water samples during the measurement. Thus calibration was made after the measurement period. We chose moments when SSC changes were obvious and took seven water samples from water surface layer and, at the same time, five OBSs were bound together and put into water at the same depth to record the turbidity. Laboratory calibration results confirmed a linear relationship between measured turbidity and SSC with a correlation coefficient lager than 0.9.

3.3. Data processing and analytical method

In the bottom boundary layer, the vertical velocity structure is considered to be logarithmically distributed, and can be described by Karman-Prandtl model (Dyer, 1986):

$$u = \frac{u_*}{\kappa} \ln \frac{z}{z_0} \tag{1}$$

where u is the measured velocity at level z above the seabed; z_0 is the bed roughness length, κ is van Karman's constant generally taken as 0.4; u_* is the friction velocity, and the bed shear stress can be related to u_* using the following equation:

$$\tau = \rho {u_*}^2 \tag{2}$$

where ρ is the density of sea water, which is taken as 1.025×10^3 kg/m^3 here. Equation (1) can be used to calculate u_* of each time interval by fitting measured velocity u and $\ln z$ to a linear relationship, u_* is obtained through the slope of the line.

In this study, high resolution and high-frequent velocity data obtained by "Vectrino Profiler" were filtered using controlling parameters of Signal to Noise Ratio (SNR) and Correlation. As for ADCP data, corresponding software was used to get the data after filtering. To eliminate the influence of fluctuation, one minute averaged velocity data (each of them is called a "burst") were used in the following analysis.

Bottom boundary layer thickness on tidal flats is suggested to be the same magnitude as water depth (Nielsen, 1992; Gao, 2010). To investigate the near bed flow structure herein, only near bottom velocities within 55 cm were used to do the fitting and the correlation coefficient was checked at the 95% confidence level. The fitting range was in the bottom boundary layer, thus the velocity profile could be adequately represented by a logarithmic profile and the calculated values of u_* are ensured to be reliable.

4. Results

4.1. Hydrodynamic processes and suspended sediment concentrations

Water depth, significant wave height and flow speed at 3 cm above the sea bed of the observation point A during three tidal cycles are shown in Figure 3. During one tidal cycle, the time of submergence ranges between 6.6-7 hours while the time of emergence is 5.3-5.6 hours (Figure 3b). After the flat surface was submerged, the average duration of the flood tide is 3.47 hours,

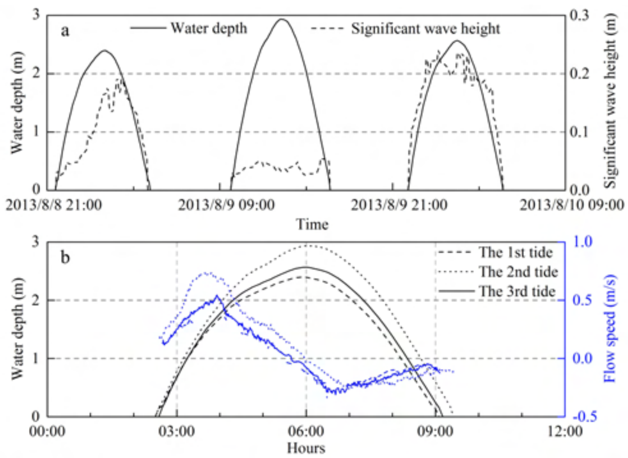

Figure 3: (a) Time series of water depth and significant wave height on study site (Station A in Figure 1b) during observation; (b) water depth and flow speed at 3 cm above the sea bed measured over three tidal cycles. Speed data of the first tidal cycle is discontinuous because there was a problem with the data acquisition software of "Vectrino Profiler".

which is a little longer than the ebb tide duration of 3.25 hours. During these observations, the prevailing wind direction was south to southwest, the maximum wind-speed and induced wave height were 6.1 m/s and 0.25 m, respectively. In this study, the second tide was selected to be analyzed, because waves during this tide were the weakest and the significant wave height was mostly less than 0.055 m. They had minor effect on the tide-induced bottom boundary layer.

Figure 4a shows the variation of water depth and near bottom velocity (3 cm above the mud surface) of the second tidal cycle on August 9. Flood tidal currents arrived at the study site (Station A) at about 9:45, and the subsequent ebb tidal flow left at about 16:45, thus the total time of submergence is 7 hours. The slack water at the end of flood occurred at around 13:15 when water depth reached the maximum and lasted for about eight

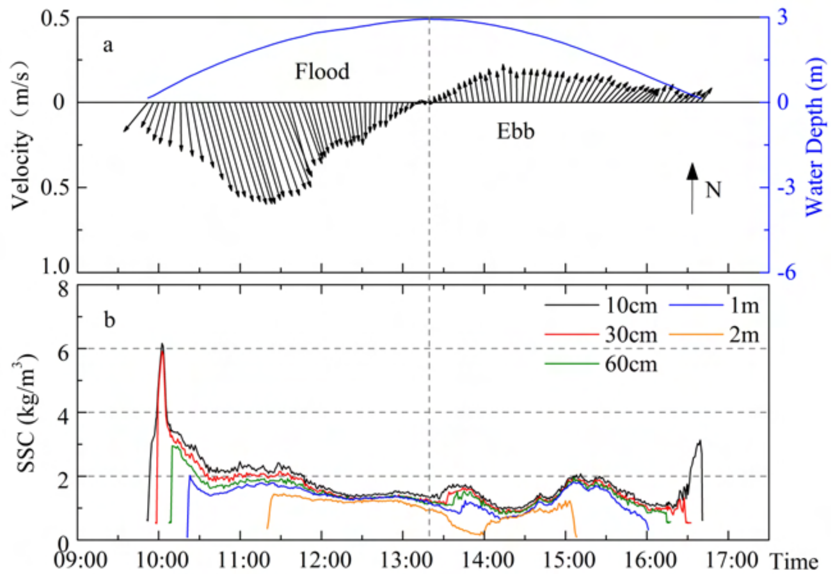

Figure 4: (a) Water depth and velocity vector at 3 cm above the mud surface; (b) Stratified suspended sediment concentration process of the second tidal cycle.

minutes.

The main flow direction is 160° − 220° during the flood phase and 240° − 60° during the ebb phase, indicating a rectilinear flow approximately parallel to the coastline. Influenced by local topography, the flow direction was nearly perpendicular to the shoreline at the beginning of the flood and the end of the ebb. The tidal asymmetry is quite evident during a tidal cycle. Although the duration of flood and ebb period is nearly the same, the maximum flood velocity (0.80 m/s) is almost twice larger than the maximum ebb velocity (0.28 m/s). Water fluxes during the flood tide are greater than that during the ebb tide and the net water flux during one tidal cycle tends to be alongshore.

The temporal variation of SSC during one tidal cycle is illustrated in

Figure 4b. There is a clear phase lag of about half an hour between the sediment concentration and the flow velocity processes.

With the arrival of the tidal front, sediment was suspended rapidly and the near-bottom SSC surged to the peak value of 6.15 kg/m^3, which tended to be the maximum value during the whole tidal cycle. However, after the front passed, part of the coarse grained suspended sediment deposited back to the bed. The subsequent flow was not strong enough to re-suspend the coarser sediment. Thus, the suspended sediment concentration decreased to about 2 kg/m^3 instead. Around the flood slack moment at 13:15, the tidal current turned direction and the flow velocity fluctuated around zero. Because of the slack period, the suspended sediment showed a depositional trend from 13:30 to 14:00, for the concentration in the surface layer decreased while increased in the lower layer. In the subsequent ebb tide, the lower sediment concentration rose up again to 3.13 kg/m^3 when the water level fell to 0.13 m, producing a second large value of SSC during the whole tidal cycle.

During most of the time, the suspended sediment in the water column was well-mixed vertically, except for the slack period when the vertical SSC gradient increased and the suspended sediment-induced vertical stratification was noticeable.

4.2. Structure of near bottom velocity profile

Stratified velocities within 10 cm and beyond 35 cm above the flat surface were measured by the "Vectrino Profiler" and RiverRay ADCP, respectively. Those of seven layers are illustrated in Figure 5b. The measured velocity profiles below 55 cm near the bed were used to explore the near bottom flow structure, and were further fitted using Equation (1). Because of the bed deformation (shown by the black dots in Figure 5c), the height of the measured velocity profile from the flat surface (i.e. parameter z in equation (1)) was changing. Real-time heights of the velocities were used to do the fitting. In addition, in this study, the velocity profile is considered to be logarithmically distributed when the correlation coefficient exceeds 0.95.

The correlation coefficients (r) of fitting results are shown in Figure 5a, in which the blue dots correspond to $r \geq 0.95$ and the red ones $r < 0.95$. Overall, 392 out of 408 (about 96%) velocity profiles can be represented by a logarithmic relationship.

Figure 5d illustrates the measured velocity profiles (the red dots) and the fitting curves (the blue lines) at five typical moments: the initial flood (burst 2), the flood peak (burst 70), the flood slack (burst 205), the ebb peak (burst 278) and the end of ebb (burst 408). As shown in burst 205, profiles around the slack period deviate from the logarithmic profile. This is attributed to the special characteristic of bidirectional flow during reversing moment, which is not considered as the focus of this study. In the following analysis, only those profiles that followed a logarithmic distribution were used to calculate bed shear stress.

4.3. Bed shear stress and bottom deformation

Bed shear stress is a frictional drag exerted at the sediment-water interface. It is a key parameter to evaluate the sediment erosion, deposition and transportation. Based on the logarithmic fitting method, bed shear stress calculated by equation (2) is shown in Figure 5c.

The calculated bed shear stress correlates well with the measured velocity, and the asymmetry is more pronounced. The maximum value of the

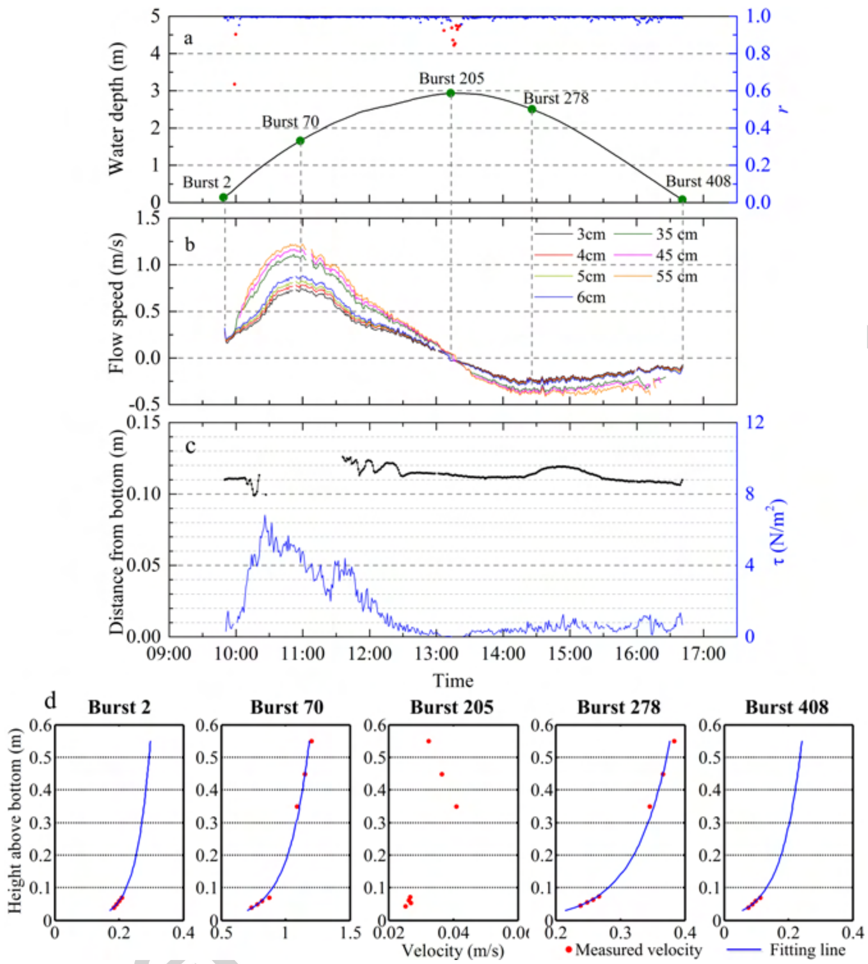

Figure 5: (a) Water depth and correlation coefficients (r) of the logarithmic fitting. The blue dots correspond to $r \geq 0.95$ and the red ones $r < 0.95$ using velocity profiles within the height 55 cm above the bottom ; (b) Stratified flow speed used for fitting (the velocity during the flood is positive while that during the ebb is negative); (c) Calculated bed shear stress and bottom deformation at the study site. The black line illustrates the change of distance from the transducer of "Vectrino Profiler" to the flat surface, data obtained from 10:22 to 11:35 is not shown because the instrument misjudged the boundary due to high suspended sediment concentration near the bottom; (d) Measured velocity profiles and fitting lines at five typical moments represented by the green dots in panel (a).

bed shear stress reaches 6.82 N/m^2 during the flood period with an average value of 2.53 N/m^2. During the ebb period, the average value is only 0.52 N/m^2, which is almost one order of magnitude smaller than the average value during the flood period. However, it is worth noting that except for the two peaks at the beginning of the flood and end of the ebb, the maximum SSC during the flood and ebb does not vary significantly (Figure 4b). The source of suspended sediment may be responsible for this phenomenon. It is known that both local re-suspension and advection contribute to suspended sediment concentration (Yu et al., 2012). The suspended sediment at the study site is predominantly advection, with a small contribution from local re-suspended sediment. Thus the total amount of suspended sediment is not so sensitive to bed shear stress.

In addition, bottom deformation was recorded by the "Vectrino Profiler" and the distance from the transducer to flat surface is illustrated by the black line in Figure 5c. Data obtained from 10:22 to 11:35 is not shown because the instrument overestimated the bed level due to high suspended sediment concentration near the bottom. Overall, the result after processing shows a positive correlation with bed shear stress and visually reflects the influence of hydrodynamics on geomorphologic changes. As the bed shear stress increased, the bed was eroded significantly soon afterwards, and vice versa.

5. Discussion

5.1. Interactions between hydrodynamics and SSC during observed very shallow water periods

The initial period of the flood and the latter period of the ebb are the two stages with very shallow water. However, due to the limitation of the mounting height of the instruments (Figure 2c), velocity and SSC data was available only when water depth was larger than 10 cm.

The relationship between the recorded velocities (or SSC) at different layers and water depth above the mudflat surface is illustrated in Figure 6. Surges can be found in velocity and SSC variations during both periods. The surge phenomenon was clearly identified in the SSC record whilst the velocity surge was only recorded in the latter stage of the tidal front. When the water was only 15 cm deep, the velocity of the tidal front reached 32 cm/s (indicated by the orange arrow in Figure 6a) and the corresponding bed shear stress was 1.5 N/m^2 (Figure 5c). As the critical incipient velocity for local bed load is about 0.15 m/s (from laboratory experiment), fine sediments deposited at the end of the last tidal cycle were re-suspended rapidly under the strong action of the tidal front. The SSC at 10 cm above the bottom surged dramatically (indicated by the orange arrow in Figure 6b). However, there is a time lag between the initial velocity surge and the subsequent SSC peak due to the "scour lag" (Postma, 1961; Friedrichs, 2011) or "diffusion lag" effect (Yu et al., 2011). The water depth had increased to 40 cm when the SSC reached its peak of 6.15 kg/m^3. The sediment-laden flow mixed well vertically at this moment, thus the SSC at 10 cm and 30 cm height were almost the same. In this short process, the suspended sediment concentration responded to

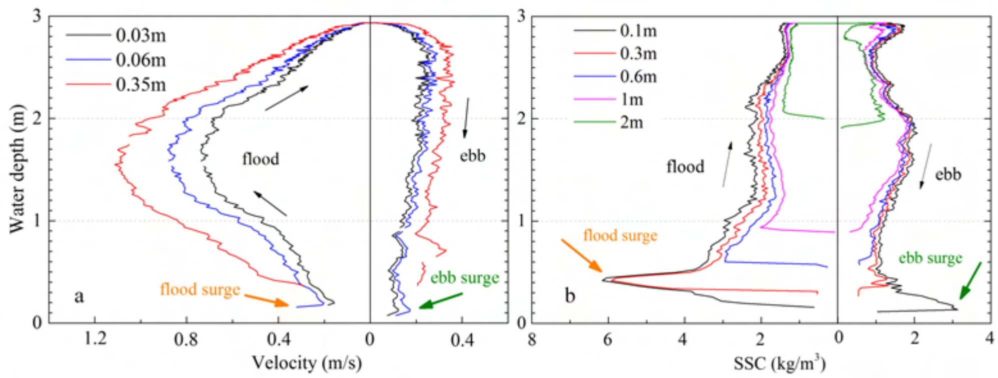

Figure 6: The relationship between (a) stratified velocity and water depth; (b) stratified SSC and water depth during flood and ebb periods of the second tidal cycle. Surge phenomena (indicated by the orange and green arrows) are evident at the very shallow water stages, especially for SSC process.

the hydrodynamic condition sensitively, which strongly indicates a dominant contribution of local sediment suspension to the total turbidity of the water. After the tidal front passed, the water depth continued to grow and the SSC gradually dropped, with a proportion of the sediment depositing on the mudflat surface. The bottom deformation process in Figure 5c offers an intuitive impression of this process, as the distance from the transducer of "Vectrino Profiler" to the flat surface had an evident decrease at about 10:15. The tidal front only lasted for a short time; about three minutes for the velocity surge and seven minutes for SSC surge (larger than 4 kg/m^3).

At the end of ebb when water depth dropped below 0.4 m, the velocity increased gently (indicated by the green arrow in Figure 6a). Although the velocity did not rise significantly, bed shear stress surged from 0.2 N/m^2 to 1.4 N/m^2 (Figure 5c). Simultaneously, SSC exhibited a marked increase to 3.13 kg/m^3 (indicated by the green arrow in Figure 6b), and the water depth decreased close to 10 cm at this moment. In such a very shallow water environment, tidal flow is thought to be enhanced by reverse osmosis water (Bassoullet et al., 2000; Gao, 2010) and leads to a slight increase in velocity.

Additionally, the very shallow flow can be more considerably influenced by the bottom friction. Figure 7a-b shows a time sequence of velocity profiles near the bottom in both of these two very shallow water periods. As shown in Figure 7a, the velocity gradient was the largest at 9:50 (the water depth was 15 cm at this time). In the following five minutes, the velocity gradient showed a descending trend as the tidal level increased. For the later ebb period, this trend was even more obvious (Figure 7b). In general, the gradient of vertical velocity gets larger when the water depth gets smaller, which indicates a larger bed shear stress.

5.2. Reconstruction of the very shallow water conditions

Figure 8 shows two site photos of the tidal front at the first sight from different angles and two boundaries can be clearly seen. The red dashed line indicates the border between emerged tidal flat surface and tidal front water. Flood flow propagates to the upper part of the tidal flats smoothly at the study site, with no breaking water on the tidal wave front. Such a front differs from the "tidal bore" phenomenon reported by Gao (2010), which is determined by the local hydrodynamic and geomorphological condition. The coordination between large velocity and very shallow water is necessary for a "tidal bore" to happen (Xu and Wang, 1998; Gao, 2010). The flow velocity of the tidal front at our study site is probably still not sufficient to produce the "tidal bore". The green dashed line is the boundary between relatively clear water and highly turbid flow. The "scour lag" effect may contributes to

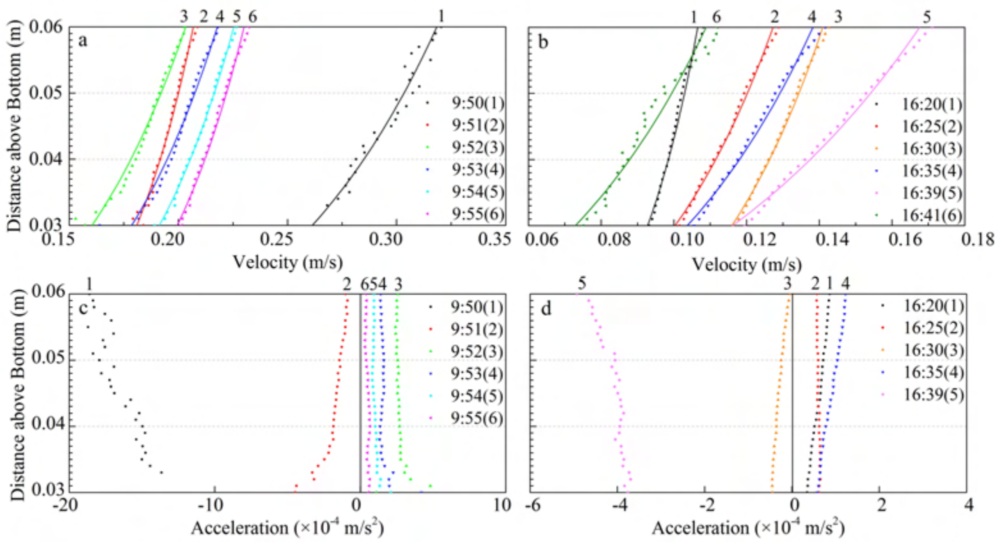

Figure 7: (a) Velocity profiles and the logarithmic fitting lines in time sequence during the initial stage of flood and (b) at the end of ebb. Both of them indicates larger velocity gradient when water depth gets smaller. (c) Acceleration profiles in time sequence corresponding to the same periods as the velocity profiles during the initial stage of flood and (d) at the end of ebb. Each acceleration is obtained between the velocity of interest and the one following.

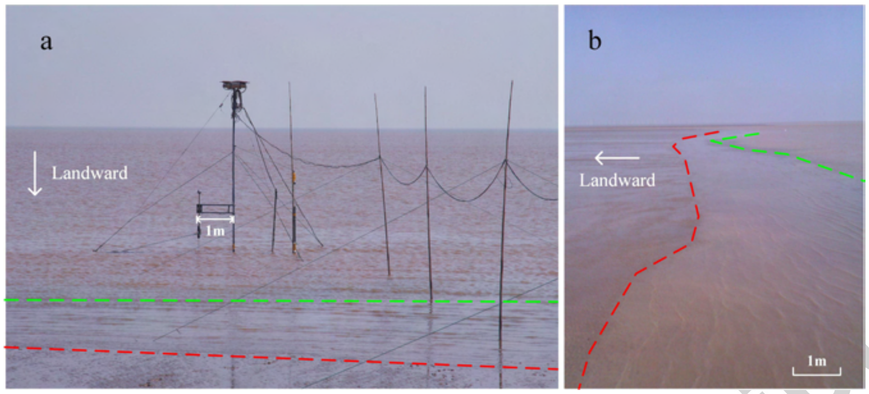

Figure 8: Site photos of (a) the front view and (b) the side view of the tidal front; two boundaries can be clearly seen in these two photos, one (the red dashed line) is the border line of flat surface and tidal front water, the other (the green dashed line) is the boundary of relatively clear water and following turbid flow.

a phase lag of sediment suspension responding to flow velocity. Additionally, it seems to indicate an acceleration process of the front flow. When the tidal flats start to be inundated, the front flow is too weak to suspend the surface sediments. With the rise of water depth and the arrival of stronger tidal current, disturbed sediments are suspended quickly and the first SSC peak is produced as shown in Figure 4b. As a result, the overlying sediments on the mudflats are not stirred immediately as the front water flows over, and there is relatively clear water zone for a short period.

According to the water depth variation shown in Figure 4a, the rate of the water level change is estimated to be 3×10^{-4} m/s at both the beginning of the flood and the end of the ebb. Under such a changing rate of water level (which is assumed to change little in several minutes), the study site is supposed to have been wetted for about five minutes before the instruments began to work (i.e., for water depth increased from 0 to 10 cm). The duration is the same after the instruments stopped working while the tidal flat was still inundated.

What has happened during these extra five minutes that were unrecorded?

To explore the velocity variation trend during the unrecorded periods, the acceleration profiles were plotted in Figure 7c-d. Each acceleration is obtained between the velocity of interest and the one following. The initial deceleration (profile 1 and 2 in Figure 7c) highlights the fact that the flow velocity was potentially even faster before the water depth was sufficient for it to be measured by the "Vectrino Profiler". Since the tidal front is nearly landward (Figure 4a), and hence normal to the shore, a deduction of the initial speed at which the front propagates across the tidal flats can be made. The slope of the mudflats in the study site is about 0.06% (Gong et al., 2014), and the rate of water level change is considered to be 3×10^{-4} m/s at the beginning of the tide. Based on the mass conservation theory, the horizontal spreading velocity of the tidal front is estimated to be 0.5 m/s, which is higher than the first recorded velocity of the flood surge. Whilst this ignores the effects of friction and any free surface gradient, it does provide a first order estimate to bound the problem.

In numerical modeling, wetting and drying is a classic problem. Modelers typically use a cut off depth below which the flow velocity is considered to be zero. It is assumed that the tidal wave has some minimum depth to maintain the front, and the speed can be estimated by $\sqrt{gh}$ where h is the water depth at the front. According to the above deduction, the critical depth to maintain the front velocity (0.5 m/s) is about 0.025 m.

During the extra five minutes in the ebb phase, the negative acceleration of profile 5 (Figure 7d) indicates a continuously decreasing trend of the flow velocity. Limited data shows that the velocity at 16:39 was the largest while two minutes later, the velocity fell to 0.11 m/s rapidly. It is easy to presume that the last five minutes of the ebb is a mild hydrodynamic process with small velocity, accompanied by a deposition of sediment. This is totally different from the conditions at the tidal front.

5.3. Differences of the surge phenomena in tidal creeks and on tidal flats

Previous studies (e.g., Fagherazzi et al., 2008; Hughes, 2012; Nowacki and Ogston, 2013) have reported the important characteristics of velocity surges in tidal creeks: (1) they occur when water level is at the level of the marsh surface as tidal water begins to overflow from tidal creeks to adjacent marsh surface during flood and drains from the platform into creeks during ebb; (2) their occurrence is accompanied by surges of suspended sediment concentration, producing large water and suspended sediment fluxes.

Differences of surge phenomena in tidal creeks and on tidal flats include several aspects. Firstly, the underlying mechanisms generating these two surges are different. Surges in tidal creeks are the combined effects of continuous water level change and flat-creek topography, while the rate of water level change and bottom friction are mainly responsible for surges on tidal flats. At the end of the ebb, reverse osmosis water may also enhance the ebb surge (Bassoullet et al., 2000; Gao, 2010). Secondly, the magnitude of water and sediment transport induced by surges on tidal flats is much less than that in tidal creeks. Although the SSC surge is remarkable, especially during the early flood, the water depth is relatively small and the surge process lasts only a few minutes. Consequently, the surge-induced budget of water and suspended sediment transport occupied only a small portion (approximately 1%) of the total value.

As a result, the surge-induced erosion mode in tidal creeks and on tidal flats are also different. Due to large velocity and bed shear stress, tidal creeks during very shallow water stages are undercut by strong erosive flow. This process is even accompanied with slumping of blocks of sediment from creek banks (Whitehouse et al., 2000) . Hence, velocity surge is a vital hydrodynamic factor to promote the growth and to maintain the morphology of tidal creeks. However, surges on tidal flats are much milder. They are distinguished from the "convergent flow" in tidal creeks by the lack of geomorphic constraint. The resulting erosive effect on morphology is relatively small and slow. It is more exact to say that the surge flow "sculptures" micro-bedform compared with obvious scour process found in tidal creeks. Actually, it is quite significant because the surge contributes to a large spatial scale of micro-topography change, which will influence the overall bed roughness and the near-bed vertical flow structures.

5.4. Linking surges with micro-topography

The importance of the surges on tidal flats is remarkable. Although the tidal front only lasted for a short time: some three minutes for velocity surge and seven minutes for SSC surge (larger than 4 kg/m^3), its function in sediment incipient motion has a profound impact on the following sediment transport. Meanwhile, since the surge-induced bed shear stress is still larger than the critical bed shear stress, surface sediment can be suspended and transported by the sheet flow.

Figure 5c implies bed erosion during the very shallow water stages. In the beginning of the flood tide, possible erosion caused by the tidal front was not recorded due to mounting height limitation of the "Vectrino Profiler". As the tidal front passed, a significant deposition has been observed, indicating a high sediment-carrying capacity of the tidal front current and a decreasing strength of the following flow. During the ebb surge, there was a potential erosion indicated by the sudden increase of the distance around 16:40 in Figure 5c. However, the instrument was exposed to air before providing more direct evidence of bed deformation. After the tidal flat exposed, sand ripples can be found everywhere, which were approximately 1-2 cm in height and 5-10 cm in length (Figure 9a). Notably, the shape of the sand ripples were highly asymmetric with the wave crest nearly "cut" by the flow. This type of sand ripple was also recorded by Gao (2010), which is supposed to be the product of the very shallow water. He also suggested that during the latter ebb period, the bed form would be gradually flattened (illustrated by the cartoons in Figure 9c-e) by the shallow flow and finally evolved into plane bed under certain conditions. However, more direct evidences (e.g. the critical shear stress for erosion and the bed shear stress of the "sheet flow") during the very shallow water period still need to be collected to explore the substantial process and to quantitate the contribution of the very shallow water to the micro topography evolution.

Meanwhile, small grooves may be produced with some disturbance, such as shells and gravels. Furthermore, small scale morphological change may lead to local flow convergence, and this is one of the major incentives of tidal creek formation (Zhou et al., 2013, 2014).

The contribution of the very shallow water to the micro-topography is

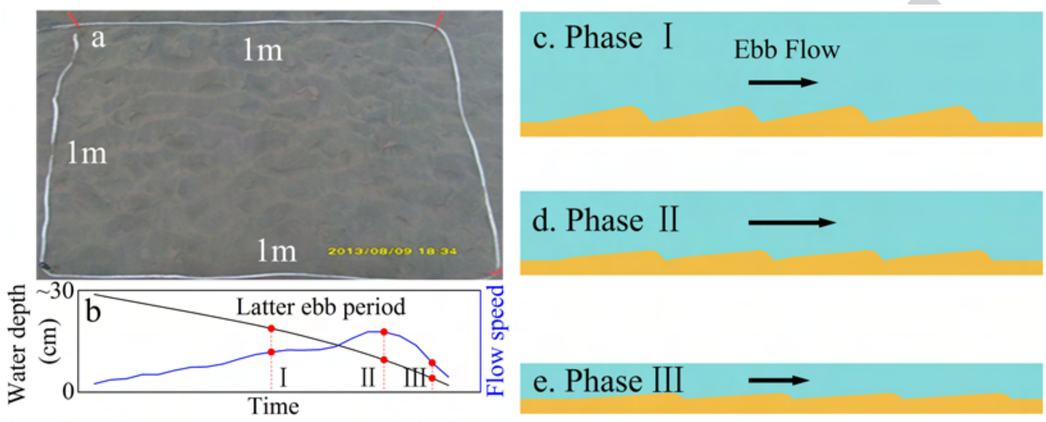

Figure 9: (a) Scaled site photo of the local sand ripples, with the wave length approximately 5-10 cm and the height 1-2 cm; (b) Schematic diagram of the water depth and the flow speed during the latter period of the ebb; (c)-(e) are cartoons illustrating the evolution of the sand ripples under the ebb tidal currents. Under certain conditions, the wave crests of the sand ripples were "top-cutted" by the "surged" shallow flow at the end of the ebb. Finally, the sand ripples would be nearly "sculptured" into plane bed. The whole process may last for more than 30 minutes.

convinced, while the interaction mechanism between hydrodynamics and micro-topography is still not well understood, primarily because the hydrodynamic and sediment condition near the bottom are difficult to measure. The capability of instruments that can be deployed in the field continues to improve, opening up new opportunities for more intense monitoring of a range of processes. This should be of particular benefit to modelers, as it should enable better representation and parameterization of such processes, as well as a more direct link between field measurements and model abstractions.

6. Conclusions

Based on the high-resolution field measurement of flow velocities and suspended sediment concentrations within 3-6 cm from the tidal flat surface, we analyze the characteristics of near-bed flow and the response of sediment and micro-topography to hydrodynamic conditions in very shallow water environments and the following conclusions are drawn:

(1) The studied tidal flat is strongly flood-dominated and characterized by a net alongshore water and sediment fluxes;

(2) Within 55 cm above the bed, the vertical structure of velocity profiles maintains a logarithmic distribution during the whole tidal cycle, except for the slack water periods;

(3) The very shallow water environment on tidal flats includes a transient phase at both the initial stage of the flood and the last stage of the ebb;

(4) During these two stages, tidal flows are very shallow with a water depth in an order of 10 cm, but large in velocity gradient and suspended sediment concentration;

(5) Evident "surge" phenomena in both velocity and suspended sediment concentration were observed. They did not occur at the same time, nevertheless they are all products of the very shallow water effect.

(6) The observed velocity of the tidal front reached 32 cm/s and the induced instantaneous sediment concentration was as high as 6.15 kg/m^2;

(7) The velocity of the tidal front is inferred as 0.5 m/s, which is larger than the first recorded velocity of the flood surge. However, the flow at the end of ebb continuously decelerated after the measurement stopped.

Compared with the surge phenomena in tidal creeks, surges on tidal flats are transient and relatively small-scale processes, which may contribute little to the whole water and sediment budgets. However, the resulting bed shear stresses of the surges appear to be sufficient to re-suspend and transport sediment, and hence play an important role on the formation and evolution of micro-topographies on tidal flats.

Acknowledgements

We would like to thank Cai Hui, Zhu Shanpeng, for their concerted efforts in technical support, instruments deployment and sediment sampling. We also acknowledge the help provided by Wang Jie and Xie Jie in laboratory experiments. Additional thanks go to Dr. Zhou Zeng (University of Cantabria) for his constructive comments. Wind data used in this study were provided by the experiment center of the college of harbor, coastal and offshore engineering, Hohai University. This work was supported by the National Natural Science Foundation of China (51379003, 51179067), the Fundamental Research Funds for the Central Universities (2015B15814, 2015B25614, 2015B24814) and also supported by Program for New Century Excellent Talents in University (NCET-12-0841).

References

Allison, M. A., Nittrouer, C. A., and Kineke, G. C. (1995). Seasonal sediment storage on mudflats adjacent to the amazon river. *Marine Geology*, 125(3C4):303–328, doi:10.1016/0025-3227(95)00017-S.

Bassoullet, P., Le Hir, P., Gouleau, D., and Robert, S. (2000). Sediment transport over an intertidal mudflat: field investigations and estimation of fluxes within the "baie de marenngres-oleron" (france). *Continental Shelf Research*, 20(12-13):1635–1653, doi:10.1016/S0278-4343(00)00041-8.

Bayliss-Smith, T. P., Healey, R., Lailey, R., Spencer, T., and Stoddart, D. R. (1979). Tidal flows in salt marsh creeks. *Estuarine and Coastal Marine Science*, 9(3):235–255, doi:10.1016/0302-3524(79)90038-0.

Boon, J. (1975). Tidal discharge asymmetry in a salt marsh drainage system. *Limnology and Oceanography*, 20(1):71–80.

Carling, P. A., Williams, J. J., Croudace, I. W., and Amos, C. L. (2009). Formation of mud ridge and runnels in the intertidal zone of the severn estuary, uk. *Continental Shelf Research*, 29(16):1913–1926.

Dyer, K. R. (1986). *Coastal and estuarine sediment dynamics*. John Wiley and Sons.

Fagherazzi, S., Hannion, M., and D'Odorico, P. (2008). Geomorphic structure of tidal hydrodynamics in salt marsh creeks. *Water Resources Research*, 44(2), doi:10.1029/2007WR006289.

Fagherazzi, S. and Mariotti, G. (2012). Mudflat runnels: Evidence and importance of very shallow flows in intertidal morphodynamics. *Geophysical Research Letters*, 39(14):L14402, doi:10.1029/2012GL052542.

French, J. R. and Stoddart, D. R. (1992). Hydrodynamics of salt marsh creek systems: Implications for marsh morphological development and material exchange. *Earth Surface Processes and Landforms*, 17(3):235–252, doi:10.1002/esp.3290170304.

Friedrichs, C. T. (2011). Tidal flat morphodynamics: A synthesis. *Treatise on Estuarine and Coastal Science*, 3:137C170, doi:10.1016/B978-0-12-374711-2.00307-7.

Gao, S. (2010). Extremely shallow water benthic boundary layer processes and the resultant sedimentological and morphological characteristics (in chinese). *Acta Sedimentologica Sinica*, 28(5):926–932.

Gong, Z., Jin, C., Zhang, C., Li, H., and Xin, P. (2014). Surface elevation variation of the jiangsu mudflats: field observation (in chinese). *Advances in Water Science*, 25(6):880–887.

Gong, Z., Zhang, C., Tao, J., and Cai, H. (2013). Mechanisms for the evolution of double-convex cross-shore profile over accretional mudflats (in chinese). *Advances in Water Science*, 24(2):212–219.

Healey, R. G., Pye, K., Stoddart, D. R., and Bayliss-Smith, T. P. (1981). Velocity variations in salt marsh creeks, norfolk, england. *Estuarine, Coastal and Shelf Science*, 13(5):535–545, doi:10.1016/S0302-3524(81)80056-4.

Hughes, Z. J. (2012). Tidal channels on tidal flats and marshes. In Jr., R. A. D. and Dalrymple, R. W., editors, *Principles of Tidal Sedimentology*, pages 269–300. Springer Netherlands, doi:10.1007/978-94-007-0123-6_11.

Kleinhans, M. G., Schuurman, F., Bakx, W., and Markies, H. (2009). Meandering channel dynamics in highly cohesive sediment on an intertidal mud flat in the westerschelde estuary, the netherlands. *Geomorphology*, 105(3):261 – 276, doi:10.1016/j.geomorph.2008.10.005.

Li, Z., Gao, S., and Chen, S. (2007). Characteristics of tide induced bottom boundary layers over the dafeng intertidal flats, jiangsu province, china (in chinese). *The Ocean Engineering*, 25(3):212–219.

Nielsen, P. (1992). *Coastal bottom boundary layers and sediment transport*.

Nowacki, D. J. and Ogston, A. S. (2013). Water and sediment transport of channel-flat systems in a mesotidal mudflat: Willapa bay, washington. *Continental Shelf Research*, 60, Supplement:S111–S124, doi:10.1016/j.csr.2012.07.019.

Pethick, J. S. (1980). Velocity surges and asymmetry in tidal channels. *Estuarine and Coastal Marine Science*, 11(3):331–345, doi:10.1016/S0302-3524(80)80087-9.

Postma, H. (1961). Transport and accumulation of suspended matter in the dutch wadden sea. *Netherlands Journal of Sea Research*, 1(1-2):148C180, IN1, 181C190, doi:10.1016/0077-7579(61)90004-7.

Ren, M. (1986). *Comprehensive investigation of coastal zone and tidal flat resources in Jiangsu Province (in chinese)*. China Ocean Press, Beijing.

Trowbridge, J. H. and Agrawal, Y. C. (1995). Glimpses of a wave boundary layer. *Journal of Geophysical Research: Oceans*, 100(C10):20729–20743, doi:10.1029/95JC02131.

Walsh, J. P. and Nittrouer, C. A. (2004). Mangrove-bank sedimentation in a mesotidal environment with large sediment supply, gulf of papua. *Marine Geology Material Exchange Between the Upper Continental Shelf and Mangrove Fringed Coasts with Special Reference to the N. Amazon-Guianas Coast*, 208(2-4):225–248, doi:10.1016/j.margeo.2004.04.010.

Wang, F. and Wall, G. (2010). Mudflat development in jiangsu province, china: Practices and experiences. *Ocean and Coastal Management*, 53(11):691–699, doi:10.1016/j.ocecoaman.2010.10.004.

Wang, Y. P., Gao, S., and Jia, J. J. (2006). High-resolution data collection for analysis of sediment dynamic processes associated with combined current-wave action over intertidal flats. *Chinese Science Bulletin*, 51(7):866–877, doi:10.1007/s11434-006-0866-1.

Wang, Y. P., Gao, S., Jia, J. J., Thompson, C., Gao, J. H., and Yang, Y. (2012). Sediment transport over an accretional intertidal flat with influences of reclamation, jiangsu coast, china. *Marine Geology*, 291:147–161, doi:10.1016/j.margeo.2011.01.004.

Wang, Y. P., Zhang, R. S., and Gao, S. (1999). Velocity variations in salt marsh creeks, jiangsu, china. *Journal of Coastal Research*, 15(2):471–477.

Whitehouse, R. J. S., Bassoullet, P., Dyer, K. R., Mitchener, H. J., and Roberts, W. (2000). The influence of bedforms on flow and sediment transport over intertidal mudflats. *Continental Shelf Research*, 20(10):1099 – 1124, doi:10.1016/S0278-4343(00)00014-5.

Williams, J. J., Carling, P. A., Amos, C. L., and Thompson, C. (2008). Field investigation of ridge-runnel dynamics on an intertidal mudflat. *Estuarine Coastal and Shelf Science*, 79(2):213–229, doi:10.1016/j.ecss.2008.04.001.

Xu, Y. and Wang, B. (1998). The mechanism and significance of flood surge along muddy tidal flat (in chinese). *Oceanologia et Limnologia Sinica*, (2):148–155.

Xu, Y., Wang, B., and Zhang, K. (1994). On flood surge over muddy tidal flat along the shanghai coast and its mechanism (in chinese). *Geographical Research*, 13(3):60–68.

Yang, G. S. (2001). *Coastal environment change and regional response in China (in chinese)*. PhD thesis, Nanjing Institute of Geography and Limnology.Chinese Academy of Sciences, Geography.

Yu, Q., Flemming, B. W., and Gao, S. (2011). Tide-induced vertical suspended sediment concentration profiles: phase lag and amplitude attenuation. *Ocean Dynamics*, 61(4):403–410, doi:10.1007/s10236-010-0335-x.

Yu, Q., Wang, Y. P., Flemming, B., and Gao, S. (2012). Tide-induced suspended sediment transport: Depth-averaged concentrations and horizontal residual fluxes. *Continental Shelf Research*, 34:53–63, doi:10.1016/j.csr.2011.11.015.

Zhang, C., Zhang, D., Zhang, J., and Wang, Z. (1999). Tidal current-induced formationstorm-induced changetidal current-induced recoveryinterpretation of depositional dynamics of formation and evolution of radial sand ridges on the yellow sea seafloor. *Science in China (Series D:Earth Sciences)*, 42(01):1–12, doi:10.1007/BF02878492.

Zhang, R. S. (1987). Progress of studies on sedimentary dynamics of tidal mud flat (in chinese). *Journal of Oceanography of Huanghai and Bohai Seas*, 5(2):71–79.

Zhou, Z., Olabarrieta, M., Stefanon, L., D'Alpaos, A., Carniello, L., and Coco, G. (2014). A comparative study of physical and numerical modeling of tidal network ontogeny. *Journal of Geophysical Research-earth Surface*, 119(4):892–912, doi:10.1002/2014JF003092.

Zhou, Z., Stefanon, L., Olabarrieta, M., D'Alpaos, A., Carniello, L., and Coco, G. (2013). Analysis of the drainage density of experimental and modelled tidal networks. *Earth Surface Dynamics Discussions*, 1(1):571–599, doi:10.5194/esurfd-1-571-2013.

Zhu, D., Ke, X., and Gao, S. (1986). Tidal flat sediment of jiangschinese (in chinese). *Advances in Marine Science*, 4(3):19–27.